FISEVIER

Contents lists available at ScienceDirect

Quaternary Science Reviews

journal homepage: www.elsevier.com/locate/quascirev



Decadal modulation of East Asian summer monsoon variations by external forcing and internal variability



Junji Zhu ^{a, b}, Kan Zhao ^{a, b, *}, Yongjin Wang ^{a, b}, Yingfang Cui ^c, Yijia Liang ^d, Hai Cheng ^{e, f}, R. Lawrence Edwards ^{f, a}, Xinggong Kong ^{a, b}, Xiaohua Shao ^g, Shitao Chen ^{a, b}, Lin Pang ^{a, b}

- ^a School of Geography Science, Nanjing Normal University, Nanjing 210023, China
- b Jiangsu Center for Collaborative Innovation in Geographical Information Resource Development and Application, Nanjing 210023, China
- ^c Nanjing Institute of Tourism and Hospitality, Nanjing 211100, China
- ^d College of Geosciences, Nantong University, Nantong, 226007, China
- ^e Institute of Global Environmental Change, Xi'an Jiaotong University, Xi'an 710049, China
- f Department of Geology and Geophysics, University of Minnesota, Minneapolis, MN 55455, USA
- ^g School of Geography, Nanjing University of Information Science and Technology, Nanjing 210044, China

ARTICLE INFO

Article history: Received 10 May 2022 Received in revised form 15 August 2022 Accepted 15 August 2022 Available online xxx

Handling Editor: Mira Matthews

Keywords: Stalagmite EASM ENSO Tropical volcanic eruptions Decadal timescale

ABSTRACT

Both external forcing and internal climate variability are playing significant roles in driving the East Asian summer monsoon (EASM) changes. However, dynamic linkages between these natural forcings and EASM on decadal timescales remain uncertain, partly due to the limited instrumental climate data. Here, we present a high-resolution EASM record over the past 200 years based on 2315 δ^{18} O measurements from two annually laminated stalagmites (YX92 and YX120) in Yongxing Cave over the middle Yangtze River Valley (mid-YRV). Our records match well with the δ^{18} O records from the nearby Heshang Cave, showing that EASM intensity in the mid-YRV varies at a dominant periodicity of ~80 years. The multidecadal-scale oscillations in the EASM intensity are closely related to the ENSO-like states, supporting a notion that the ENSO dominantly modulates the EASM variability. Furthermore, the decadal oscillations in EASM and ENSO are synchronous with tropical volcanic eruptions during the solar minima, probably leading to the enhanced El Niño-like response, intensified EASM and strengthened ENSO-EASM coupling. Our findings imply that external forcings potentially contribute to the anomalies in ENSO and EASM during the ongoing global warming.

© 2022 Elsevier Ltd. All rights reserved.

1. Introduction

The East Asian summer monsoon (EASM) is of critical importance for transporting moisture from the marine source to the interior of the East Asian continent. Any perturbations of the normal advance or retreat of the monsoon rain belt could lead to either deficient or excessive rainfall in summer, which could adversely affect the regional social-economic development and the well-being of the inhabitants (Ding and Chan, 2005; Zhang et al.,

E-mail addresses: zhujunji1997@163.com (J. Zhu), 09371@njnu.edu.cn (K. Zhao), yjwang@njnu.edu.cn (Y. Wang), cuiyingfang86@163.com (Y. Cui), lucy2012_2015@163.com (Y. Liang), cheng021@xjtu.edu.cn (H. Cheng), edwar001@umn.edu (R.L. Edwards), xinggongkong@njnu.edu.cn (X. Kong), xiaohua.shao@nuist.edu.cn (X. Shao), chenshitao@njnu.edu.cn (S. Chen), panglin118@163.com (L. Pang).

2008; Chen et al., 2020). Due to a great deal of uncertainty for the characteristics and causes of decadal EASM variability, however, predicting its expression remains difficult.

Observational data and model studies indicate that not only external solar and volcanic forcing (Zhang et al., 2008; Man et al., 2014; Chen et al., 2020), but also internal climate variability (Ding et al., 2018, 2020; Zhang et al., 2021), contribute substantially to the EASM and associated rainfall changes in the monsoon region of China. For example, the weakening in EASM was associated with low solar irradiance (Zhang et al., 2008) and high atmospheric aerosol concentrations as a result of volcanic eruptions (Man et al., 2014; Chen et al., 2020), and vice versa. Moreover, the volcanic eruptions during the solar activity minima had a significant impact on the precipitation distributions, caused by a widening of the Hadley Cell and a shift in the Intertropical Convergence Zone (ITCZ) (Anet et al., 2014). Due to minor changes (0.1–0.26%) in solar irradiance, the internal climate variability, such as the El Niño-

^{*} Corresponding author. Present Address: School of Geography, Nanjing Normal University, Nanjing, 210097, China.

Southern Oscillation (ENSO), Pacific Decadal Oscillation (PDO) and/ or Atlantic multidecadal oscillation (AMO), potentially provides an additional mechanism for amplifying solar signals and transmitting them globally (Clement et al., 1996; Emile-Geay et al., 2007). Meanwhile, these internal multidecadal to interannual oscillations in climate might have been driven by volcanic forcing (Brönnimann et al., 2019; Mann et al., 2021). A recent study revealed that large volcanic eruptions could promote a significantly enhanced phasesynchronization of the ENSO and Indian monsoon oscillations (Singh et al., 2020). In the EASM domain, ENSO, PDO and/or AMO have been suggested to modulate the hydroclimate variability and spatial distribution of rainfall by altering the position and strength of the Western Pacific Subtropical High (WPSH) and the westerly jet (Chiang et al., 2015; Ding et al., 2018, 2020; Zhang et al., 2021). However, the dynamic process of EASM's response to external and internal forcings is still puzzling.

Relationship between ENSO and EASM is central to summer rainfall predictions over the Yangtze River Valley (YRV). Meteorological observations indicate that changes in tropical oceanatmosphere system play a key role in affecting summer monsoon rainfall in the YRV (defined as Meiyu) on interannual and intraseasonal timescales (Ding and Chan, 2005; Ding et al., 2020). Paleoclimatic records also reveal that changes in solar activity and tropical Pacific sea surface temperature (SST) have substantial influence on centennial-scale Meiyu variations during the late Holocene (Jiang et al., 2006; Zhang et al., 2021), possibly through the "ocean dynamical thermostat" hypothesis (Clement et al., 1996). However, causes of multidecadal- to decadal-scale changes in EASM rainfall over the YRV remain unclear, partly due to the limited length of the instrumental data and/or the scarcity of high-quality hydroclimate reconstructions. Here, we present a seasonally resolved δ^{18} O record from two annually laminated stalagmites in Yongxing Cave over the middle YRV (mid-YRV), to reconstruct the history of the EASM from 1784 to 1958 AD. Synthesized with other layer-counting chronology and high-resolution stalagmite records in the mid-YRV, this study aims to explore the relevant influence of internal and external forcing on EASM variations on decadal timescales.

2. 2 Site, materials and methods

Yongxing Cave (31°35′N, 111°14′E, 800 m) is located on the east slope of Mt. Shennongjia, central China, ~150 km north of Heshang Cave (30°27′N, 110°25′E, 294 m; Hu et al., 2008a, Fig. 1a). The two cave sites are situated in the mid-YRV, which is strongly influenced by the EASM. Based on the 30-yr (1971-2000) NCEP datasets and 740 surface station data in China, EASM rainfall in the mid-YRV is dominated by the Meiyu (11th-15th June to 11th-15th July), which accounts for half of the summer rainfall (Ding and Chan, 2005; Ding et al., 2020). The large interannual variability of both the duration and the total rainfall amount of Meiyu often results in droughts or floods in the YRV, seriously affecting socioeconomic development. Based on 30-year (1981–2010) meteorological data from a nearby meteorological station (Baokang City, 31°52′N, 111°15′E; http:// data.cma.cn), the average annual rainfall is about 930 mm, 70% of which occurs during the rainy season (May to September). Cave monitoring results from June 2013 to September 2016 (Wang et al., 2018) show that the average temperature inside the cave is around 14.3 °C, slightly lower than the annual temperature outside the cave (~15.2 °C). Relative humidity inside the cave maintains ~100% all year round. The cave is developed in Silurian limestone and the thickness of the overlying host rock is ~50 m. The overlying vegetation is predominantly woody perennial plant and shrub grass.

Two stalagmites (No. YX92 and YX120) were collected in a large chamber about 100 m from the cave entrance. Samples YX92 and YX120 are 160 mm and 105 mm in length, respectively, with a 'candlestick' shape. When halved along the growth axes and polished, regular laminations can be clearly observed in the two samples, showing alternations of white-porous calcite (opaque) and dark-compact calcite (transparent) (Fig. 2a and Fig. S1). These white-dark paired laminae, with a thickness about 0.4-0.6 mm, resemble the annual laminations described by Johnson et al. (2006) and Tan et al. (2006). Cave monitoring work demonstrates that both dripping rate (faster in summer and slower in winter) and carbonate deposition amount (more in summer and less in winter) have a strong seasonality (Wang et al., 2018). Seasonal changes in climate and environment at our study site also favor the formation of the white (thick)-dark (thin) paired annual layers (Tan et al., 2006). For laminae analyses, the polished cross-sections of the two stalagmites were scanned using an EPSON4990 flatbed scanner with a 2000 dpi optical resolution. The digital images were cropped following the standard of one image per 30 mm. Visible laminae were marked and counted using Adobe Photoshop software and then lamina thickness was measured using Grapher12 software.

A total of nine powdered subsamples for ²³⁰Th dating were drilled along the growth axis of YX92 (5 subsamples) and YX120 (4 subsamples) with a carbide dental drill. The procedures for chemical separation and purification of the uranium and thorium content are similar to those described in Edwards et al. (1987). ²³⁰Th dating was performed at the Isotope Laboratory of Geology and Geophysics Department, Minnesota University, and the Institute of Global Environmental Change, Xi'an Jiaotong University. The U/Th isotopic solutions were analyzed on a Multi-Collector Inductively Coupled Plasma Mass Spectrometry (MC-ICP-MS, Neptune plus). The reported age errors are two standard deviations (2σ) (Table S1).

For stable isotope analyses, 2315 subsamples (1339 for YX92 and 976 for YX120) were collected along growing axes by knife shaving at ~0.1 mm spatial resolution, yielding 6–12 samples per lamina. The isotope measurements were conducted with a Finnigan-MAT 253 mass spectrometer coupled with a Kiel Carbonate Device in the Isotope Laboratory of Nanjing Normal University, China. All results were reported in parts per mil (‰) relative to the Vienna Pee Dee Belemnite (VPDB). Replicate analyses of an international standard (NBS19) indicated long-term reproducibility, with the precision better than 0.06‰ for δ^{18} O and 0.05‰ for δ^{13} C at the 1σ level.

3. Results

3.1. Chronology

Here, the age models of YX92 and YX120 are primarily based on annual layer counting. Based on multiple counts by different people, a total of 172 ± 12 and 157 ± 3 annual layers were counted in YX92 and YX120, respectively. Counting errors largely come from the porous sections, such as the section between the depth range of 43 mm and 109 mm in YX92 contributing to counting uncertainties of ~8 years. Because layer-counting produces a floating timescale, the chronology of the two samples must be further constrained.

The stalagmite laminae chronology was usually obtained by anchoring the floating layer-counting timescale to ²³⁰Th dates and its uncertainty was estimated by both layer-counting uncertainties and ²³⁰Th dating errors. In this study, nine ²³⁰Th dating results (Fig. 2b and Table S1) show large dating errors (11–78 yr) for the stalagmites YX92 and YX120, due to low uranium concentrations (238–455 ppb) and high initial thorium contents (108–1374 ppt). These ²³⁰Th dates are not in stratigraphic order (Table S1). In addition, correction for the effect of ²³⁰Th incorporated at the time of deposition is important, especially for young stalagmites (Richards and Dorale, 2003; Hellstrom, 2006). Any initial ²³⁰Th is

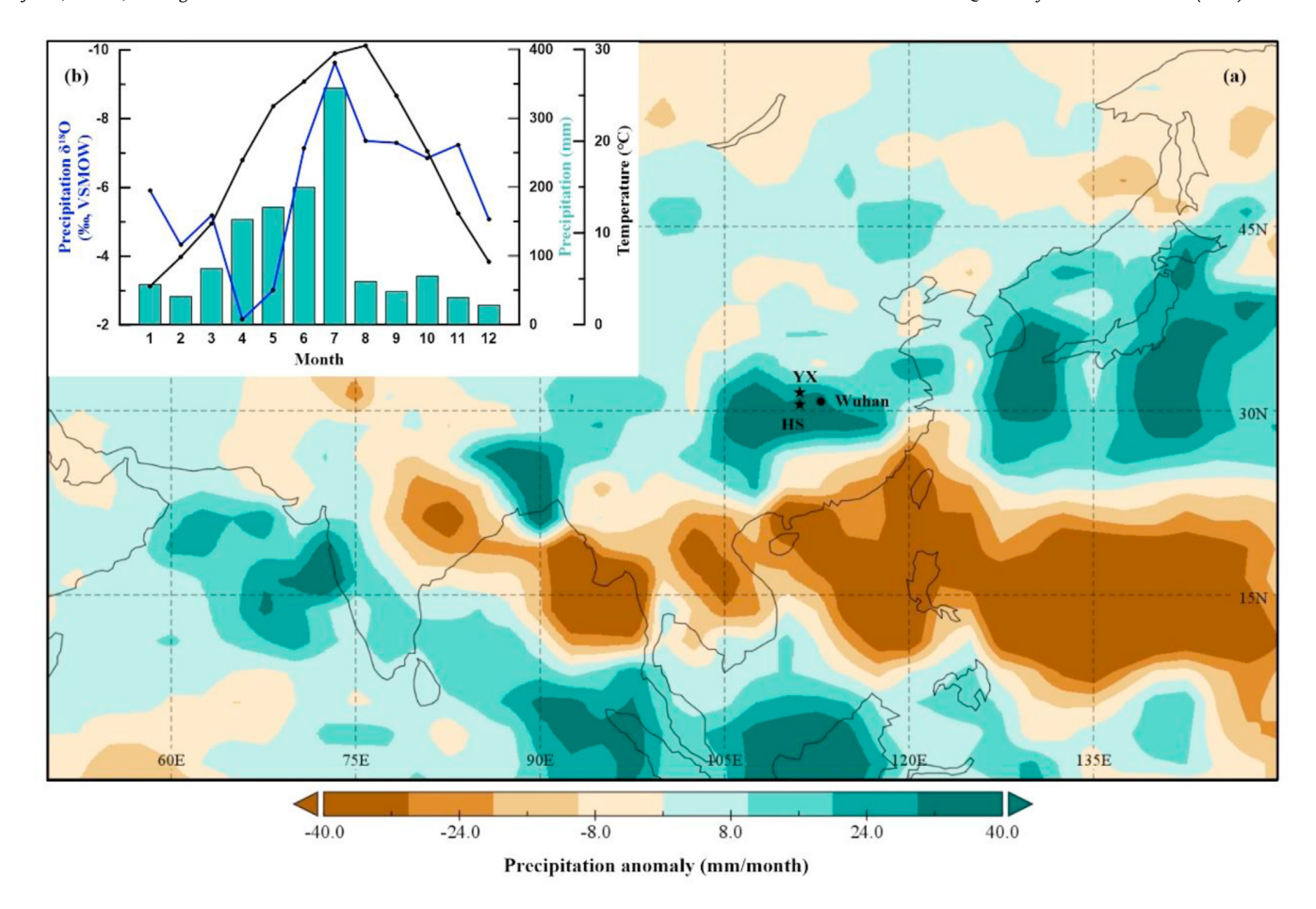


Fig. 1. Modern climatology and study sites mentioned in the text. (a) JJA (Jun-Jul-Aug) precipitation anomalies relative to the interval 1981–2010 AD during the 1982/1983, 1986/1987, 1992/1993, 1997/1998, 2006/2007, and 2015/2016 El Niño years (research data is available at: https://psl.noaa.gov/cgi-bin/data/getpage.pl); red stars indicate the cave sites (YX: Yongxing Cave; HS: Heshang Cave) and black dot shows the nearby meteorological station (Wuhan City). (b) the Wuhan meteorological data during the period of 1986–1998 AD; the data of rainfall, precipitation isotope and temperature were collected from the Global Network of Isotopes in Precipitation (GNIP) at http://www-naweb.iaea.org/napc/ih/IHS_resources_gnip.html. (For interpretation of the references to colour in this figure legend, the reader is referred to the Web version of this article.)

always accompanied by a much larger amount of ²³²Th. Therefore, ²³²Th was routinely monitored during analysis, and samples containing less than an acceptable threshold of ²³⁰Th relative to ²³²Th were objectively identified and rejected. In this study, the high ²³²Th contents with the significant initial ²³⁰Th contaminations lead to the large corrections for the 230 Th ages and excessively low 230 Th/ 232 Th atomic ratios (14 \times 10⁻⁶ to 95 \times 10⁻⁶) indicate that the correction for the initial ²³⁰Th is uncertain (Table S1; Richards and Dorale, 2003; Hellstrom, 2006). It can be also observed that the sub-samples collected at the top (YX92-26 mm and YX120-4 mm) with high ²³²Th concentrations have older ²³⁰Th ages than the subsamples at the bottom (YX92-111 mm and YX120-80 mm) with relatively lower ²³²Th concentrations (Table S1), suggesting that a greater correction for initial ²³⁰Th was required. As shown in Fig. S2, no matter which dating point is selected as the anchor point, the laminae chronology cannot be consistent with the other ²³⁰Th dates, which is largely caused by the initial ²³⁰Th uncertainties. Due to the large uncertainties of ²³⁰Th dates, it is challenging to anchor the floating layer-counting chronology via ²³⁰Th dates. Although the dating uncertainties are large, the ²³⁰Th dates still indicate that the two young samples grew during about the last 200 years.

Based on independent layer-counting chronology, the two stalagmite δ^{18} O records (YX92 and YX120) show a good replication and stable growth rates, characterized by a coherence in timing,

duration and amplitude of the decadal- to multidecadal-scale oscillations (Fig. 3 and Fig. S4). This indicates that the layer-counting results of two stalagmites are reliable to establish the laminae chronology of the δ^{18} O profiles. Therefore, we applied a method to anchor the floating timescale by comparing the $\delta^{18}O$ signals in YX92 and YX120 (Fig. 3a and b) with the stalagmite HS-4 δ^{18} O record from the nearby Heshang Cave (Hu et al., 2008a, Fig. 3c). This method is analogous to tree-ring-based stable oxygen isotope chronology by dendrochronological cross-dating (Yang et al., 2021). The reasons for choosing HS-4 record are fourfold: (a) Stalagmite HS-4 was actively growing when collected in 2001 (Hu et al., 2008a). Its annual layers are clear and verified by annual trace element and stable isotope cycles (Johnson et al., 2006). (b) The layer-counting chronology in HS-4 throughout the Holocene is essentially consistent with the U/Th chronology (Hu et al., 2008a). Based on the annual-layer-counted chronology, HS-4 record reveals a period of drying lasting 150 years (the 8200-year event) that occurred almost simultaneously with the cooling recorded by the Greenland ice cores (Liu et al., 2013). (c) The HS-4 δ^{18} O record bears a high similarity to another annually laminated stalagmite record (HS-6) from the same cave (Fig. 3c; Hu et al., 2008a). For the last 150 years, the age precision is better than 3 years (Hu et al., 2008a; He et al., 2009). (d) Heshang Cave has been extensively monitored so that the nature of the geochemical response to changing conditions

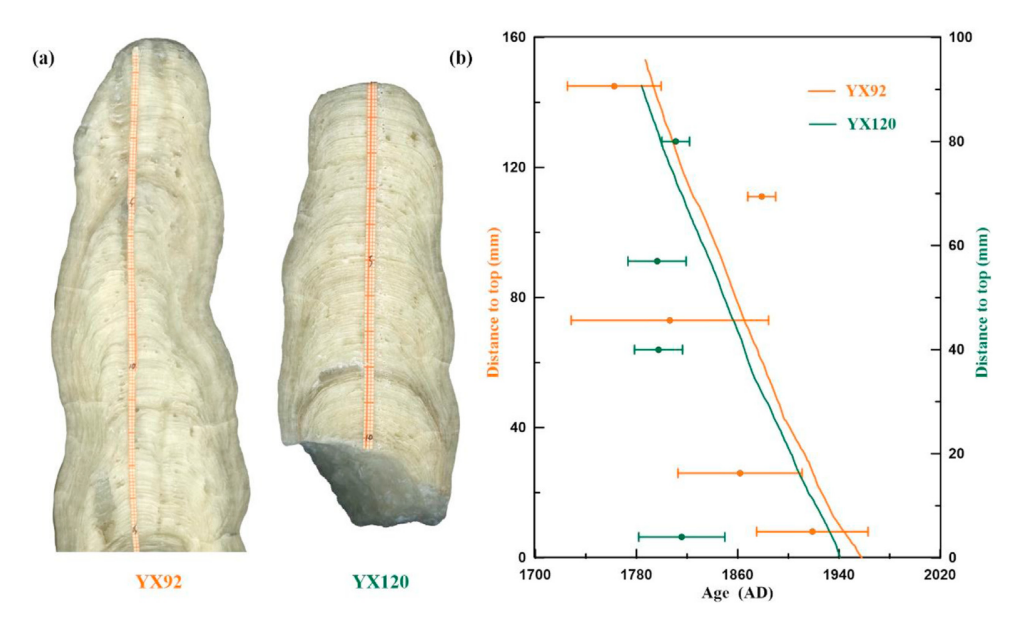


Fig. 2. Stalagmite profiles and age models of the stalagmite YX92 and YX120. (a) Polished profiles for stalagmite YX92 and YX120; (b) The age models of YX92 and YX120. The floating layer-counting timescale was constrained by comparing the δ^{18} O signals in YX92 and YX120 with the HS-4 δ^{18} O record from nearby Heshang Cave (Hu et al., 2008a). The dots and horizontal errors bars represent the 230 Th dates and dating errors (within 2σ errors) of stalagmites YX92 (orange) and YX120 (green), respectively. (For interpretation of the references to colour in this figure legend, the reader is referred to the Web version of this article.)

is well understood (Hu et al., 2008b; Duan et al., 2016). Due to a strong similarity between δ^{18} O records from Yongxing Cave (YX92 and YX120) and Heshang Cave (HS-4 and HS-6), the two YX records are anchored to the HS-4 record via anchor-point matching (Fig. 3). Two breakpoints at 1939 AD (red dot in Fig. 3c) and 1900AD (black dot in Fig. 3c) were identified in HS-4 record by using the BREAKFIT algorithm (Mudelsee, 2009). Similarly, two breakpoints (using the BREAKFIT algorithm) were identified in YX92 (1939 and 1897 AD) and YX120 (1939 and 1896 AD) records, respectively. Here, the floating timescales of the two YX records were anchored to the datum of 1939 AD (red dots in Fig. 3). Another breakpoint (1897 AD in YX92 and 1896 in YX120) in the two YX records matches well with the breakpoint at 1900 AD in HS-4 record within the counting errors, indicating that layer-counting chronologies in YX92 and YX120 records are reliable. Therefore, we determine the layercounting timescale from 1787 to 1958 AD as the best estimate for YX92 chronology and from 1784 to 1941 AD for YX120 chronology (Figs. 2b and 3), with a cumulative counting error of ± 12 and ± 3 years, respectively.

3.2. The δ^{18} O and δ^{13} C sequence

The $\delta^{18}O$ and $\delta^{13}C$ records of YX92 and YX120, with a high temporal resolution of ~1–3 months, are shown in Fig. 3, Fig. S3 and Table S2. The $\delta^{18}O$ values in YX92 and YX120 vary from -9.57% to -7.13% (~8.60% on average) and -9.62% to -7.86% (~8.77% on average), respectively. The $\delta^{13}C$ values in YX92 and YX120 vary from -12.12% to -9.3% (-10.93% on average) and -12.7% to -9.08% (-10.73% on average), respectively. Due to the uneven spacing of these $\delta^{18}O$ and $\delta^{13}C$ time series, we first resampled to adjust the time series to the lowest temporal resolution (0.25-yr) and then further to 1-yr resolution to perform the correlation and wavelet analyses. The two $\delta^{18}O$ records show a high similarity, with a correlation coefficient r=0.44 (n = 609, P < 0.01; Mudelsee, 2003). Multidecadal oscillations are evident, characterized by two

negative excursions with an amplitude larger than ~1% and a rapid transition less than 10 years (Fig. 3). Wavelet analyses of the two records show a dominant periodicity of ~80 years (Fig. S4a and 4b). The cross-wavelet analysis further confirms a coherent ~80-year cycle (Fig. S4c). Therefore, the timing, duration and amplitude of the multidecadal oscillations in the YX92 and YX120 δ^{18} O records are consistent. Due to a high similarity between YX120 and HS-4 $\delta^{18}\text{O}$ records (r = 0.64, n = 142, P < 0.01; Fig. 4a; Mudelsee, 2003) and small layer-counting errors of the two records (±3 years), we provide a composite Yongxing-Heshang (YX-HS) record covering the last 219 years (1784–2002 AD) by splicing the YX120 with HS-4 record (Fig. 4b). Systematically, the δ^{18} O values of YX120 are more negative than the HS-4 by ~0.4% (Fig. 4a), probably caused by the different elevation levels between Yongxing Cave and Heshang Cave. Therefore, the YX-HS δ^{18} O record, with the largest age uncertainty of ± 6 years, is composed of the YX120 record from 1784 to 1941 AD and the HS-4 record from 1942 to 2002 AD with a shift of 0.4% in δ^{18} O values (Fig. 4b).

Equilibrium calcite precipitation is important to interpret calcite $\delta^{18}O$ in terms of climate. The Hendy Test (Hendy, 1971) was performed on six individual growth laminae of samples YX92 and YX120 (Fig. S5). The results show that standard deviations of isotope values along the same layer are less than 0.12 for YX92 δ^{18} O (Fig. S5a), 0.16 for YX120 δ^{18} O and 0.37 for YX120 δ^{13} C (Fig. S5b), suggesting that the calcite deposited close to equilibrium. Replication is another rigorous test for isotopic equilibrium (Dorale and Liu, 2009). As shown in Fig. 3, four annually laminated δ^{18} O records from Yongxing Cave (YX92 and YX120) and Heshang Cave (HS-4 and HS-6) show good replications. The Pearson correlation coefficient between the YX120 and HS-4 δ^{18} O records reaches ~0.64 during their contemporaneous growth periods (from 1800 to 1941 AD). These observations suggest that stalagmite $\delta^{18}O$ signals from both Yongxing and Heshang caves are little affected by kinetic fractionation and can be interpreted in terms of climate (Dorale and Liu, 2009). However, the structure of multidecadal oscillations in

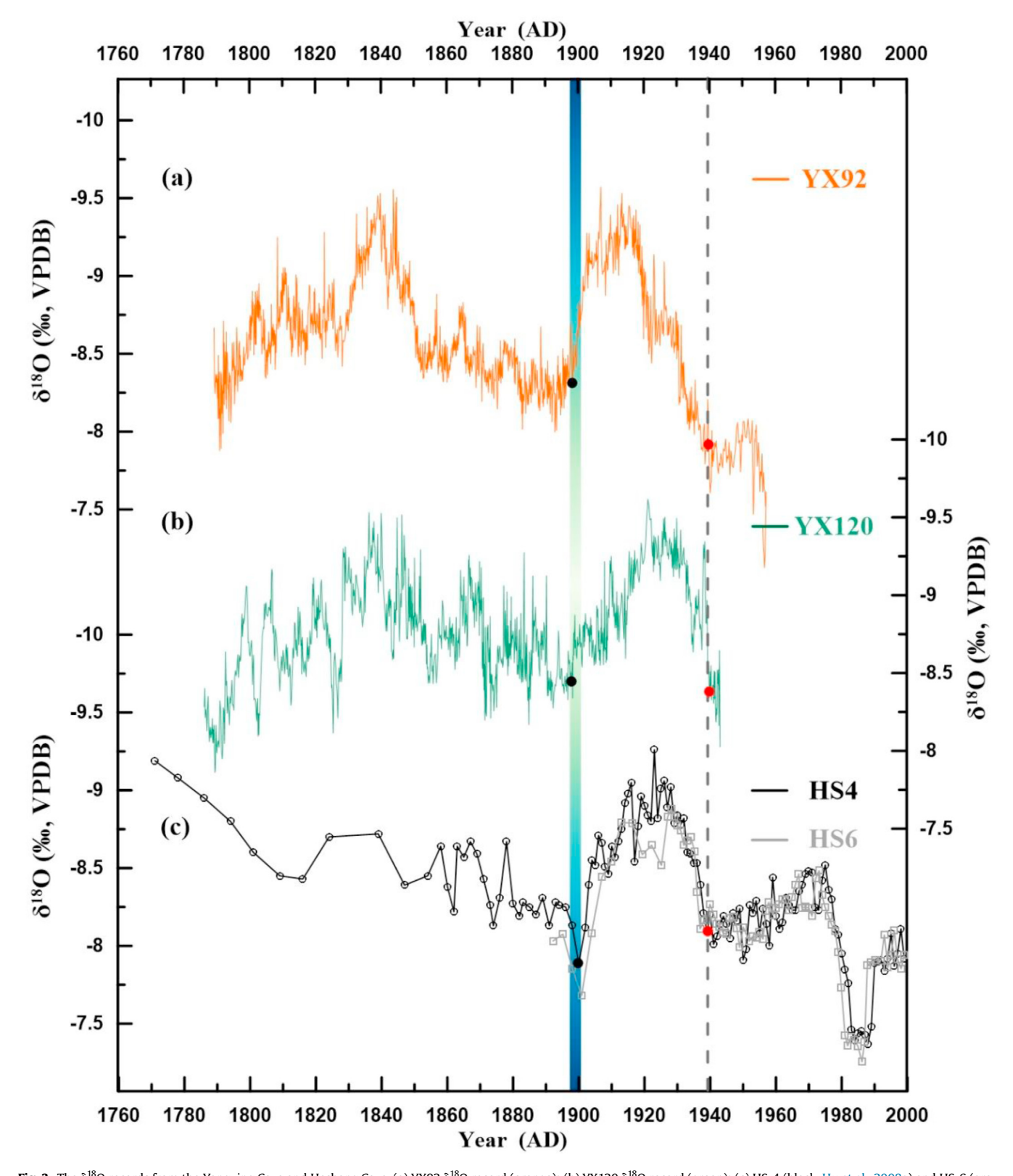


Fig. 3. The δ^{18} O records from the Yongxing Cave and Heshang Cave. (a) YX92 δ^{18} O record (orange); (b) YX120 δ^{18} O record (green); (c) HS-4 (black, Hu et al., 2008a) and HS-6 (gray, Hu et al., 2008a) δ^{18} O records. The red (right) and black dots (left) indicate the breakpoints of YX92, YX120 and HS-4 δ^{18} O records, identified by using the BREAKFIT algorithm (Mudelsee, 2009). The black dashed line shows that the three red breakpoints are synchronous at 1939 AD. The gradient blue bar denotes that the three black breakpoints (1897 AD in YX92, 1896 AD in YX120, and 1900 AD in HS-4) are synchronous within the layer-counting errors. (For interpretation of the references to colour in this figure legend, the reader is referred to the Web version of this article.)

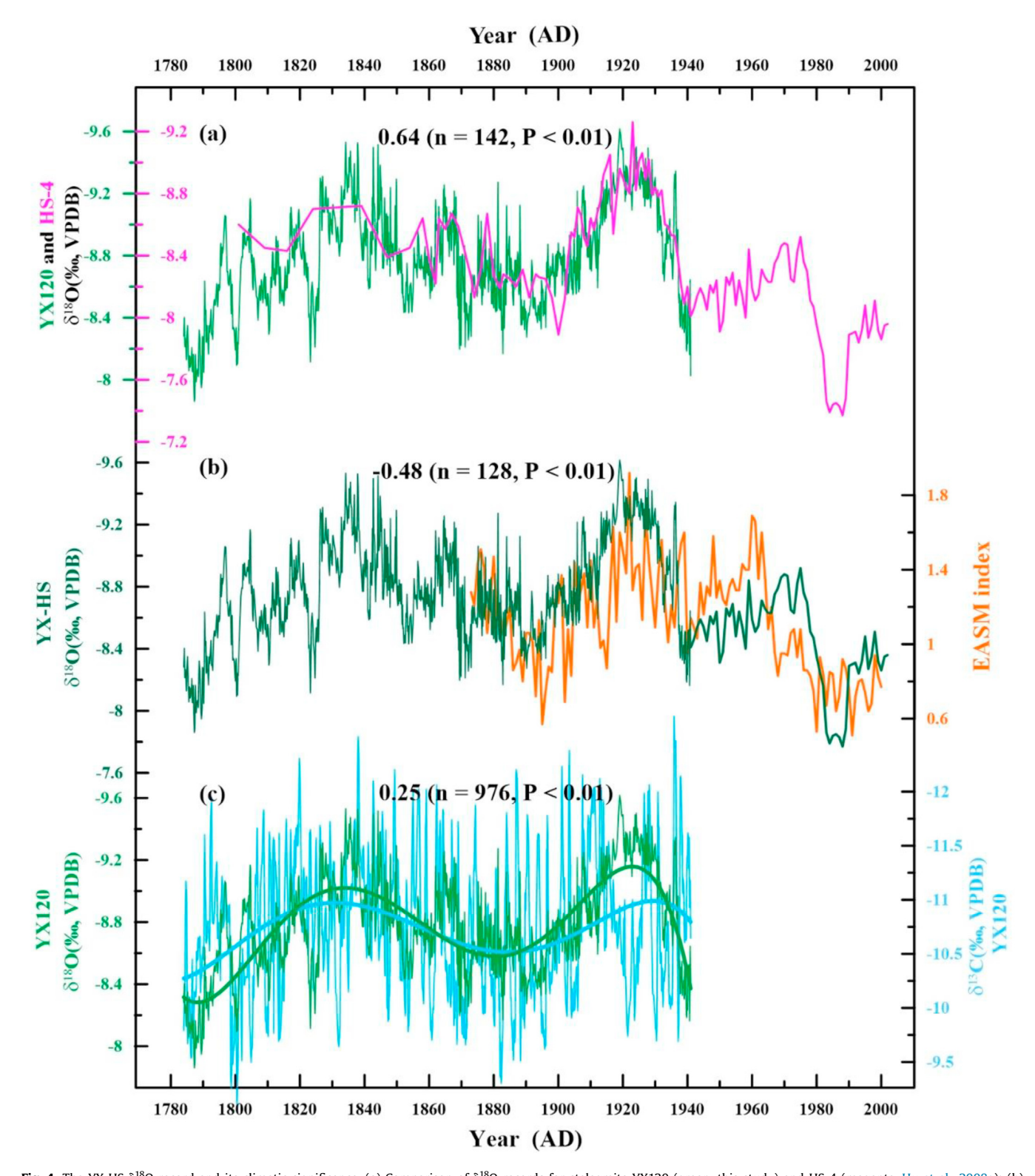


Fig. 4. The YX-HS δ^{18} O record and its climatic significance. (a) Comparison of δ^{18} O records for stalagmite YX120 (green, this study) and HS-4 (magenta, Hu et al., 2008a); (b) Comparison of the Yongxing-Heshang (YX-HS) δ^{18} O record (dark green) and the EASM index (orange, Guo et al., 2004); (c) Comparison of δ^{18} O (green) and δ^{13} C record (light blue) for YX120 and their polynomial fitting results. (For interpretation of the references to colour in this figure legend, the reader is referred to the Web version of this article.)

both YX and HS records shows slight differences, probably due to varying degrees of smoothing of the isotopic signals and different noise levels caused by a wide range of hydrological processes (e.g. drip rates, flow paths, residence time of seepage water; Duan et al., 2016; Wang et al., 2018).

4. Discussion

4.1. Interpretation of speleothem oxygen isotope and carbon isotope records

Although the climatic significance of Chinese stalagmite $\delta^{18}\text{O}$ records is still debated, recent literatures suggested that two mechanisms affect δ^{18} O: changes in the fraction of summer rainfall amount in annual totals and changes in the amount of rainout between tropical sources and cave sites (Wang et al., 2001; Yuan et al., 2004; Cheng et al., 2016). The former is caused by changes in the seasonal migration of the sub-tropical jet and likely has a smaller effect on cave $\delta^{18}O$ than the latter (Chiang et al., 2015; Orland et al., 2015). The latter involves changes in rainout from both the Pacific and the Indian Ocean sources (Yuan et al., 2004; Wang et al., 2020; Liang et al., 2020). For both, lower δ^{18} O implies higher spatially integrated monsoon rainfall between the tropical monsoon sources and the cave site and/or higher summer monsoon rainfall in the EASM region (Cheng et al., 2016; Liang et al., 2020). Thus, in this study, we use the terms 'strong monsoon' and 'weak monsoon' to refer to low and high cave δ^{18} O, respectively, consistent with previous studies (Cheng et al., 2016; Zhang et al., 2018; Liang et al., 2020). In addition, the YX-HS δ^{18} O record bears a resemblance to the EASM index derived from instrumental sea level pressure data (r = -0.48, n = 128, P < 0.01, from 1873 to 2000 AD; Fig. 4b; Guo et al., 2004), supporting that lighter δ^{18} O values correspond to stronger EASM intensity, and vice versa.

According to modern meteorological studies, EASM rainfall over the mid-YRV is characterized by the Meiyu, involving its onset and duration (Ding and Chan, 2005; Chiang et al., 2015). As shown in Fig. 1b, local precipitation increases and precipitation δ^{18} O decreases in June as the Meiyu initiates and EASM intensifies. In term of long-term variation, instrumental data shows that Meiyu rainfall undergoes a decreasing trend since the late 1970s (Ding et al., 2020), synchronous with an increasing $\delta^{18}\text{O}$ values in both HS-4 and HS-6 (Fig. 3c, Hu et al., 2008a). Furthermore, Li et al. (2018) provided a near-annual resolution stalagmite (HS-6) record of Ca isotope compositions ($\delta^{44/42}$ Ca), as a sensitive regional hydroclimate proxy, over the last 120 years from Heshang Cave. The $\delta^{44/}$ ⁴²Ca record correlates positively with the δ^{18} O record (r = 0.36), but negatively with the instrumental summer rainfall data (r = -0.71, 10-year running mean). The $\delta^{44/42}$ Ca, δ^{13} C, Mg/Ca, Sr/Ca and Ba/Ca records in HS-4, varying in concert and in a consistent manner with regional rainfall changes, also match well with the δ^{18} O record across the 8.2 kyr event (Liu et al., 2013; Owen et al., 2016). These observations likely suggest a regional hydrological signal in stalagmite δ^{18} O records over the mid-YRV.

The stalagmite $\delta^{13}C$ has complicated factors from external conditions (e.g. variations in soil CO_2 and vegetation) and during its deposition (e.g. changes in CO_2 degassing, the drip rate of water, prior calcite precipitation (PCP)), and it can provide important information on climatic and environmental changes (McDermott, 2004; Fairchild et al., 2006). At the site of Yongxing Cave, where the modern vegetation is composed mainly of C_3 plants, the influence of vegetation on stalagmite $\delta^{13}C$ probably reflects changes in the density of vegetative cover and the biomass (Baldini et al., 2005; Fohlmeister et al., 2020). During dry conditions, reduced vegetation growth and biological activity can lead to reduced soil CO_2 production and high speleothem $\delta^{13}C$ values. Dry conditions

may also enhance PCP and lead to a longer residence time of seepage water, and greater removal of ¹²CO₂ during the degassing process, resulting in higher δ^{13} C values (McDermott, 2004; Fairchild et al., 2006; Griffiths et al., 2016). Moreover, slower drip rates are likely to allow greater CO2 degassing either at the cave ceiling or at the speleothem surface, leading to heavier $\delta^{13}C$ values (Johnson et al., 2006; Cosford et al., 2009). In general, these factors are all susceptible to hydrological changes and fluctuate in the same sense. Furthermore, the YX120 δ^{13} C record is similar to the flood/ drought index over the YRV (Jiang et al., 2006) on multidecadal to decadal timescales, with negative δ^{13} C values largely corresponding to wet conditions (Fig. S6), and vice versa. Although the YX120 δ^{13} C record displays more high-frequency oscillations than the $\delta^{18}O$ record, the two records show a broad similarity, with a correlation coefficient of 0.25 (n = 976, P < 0.01). The results of polynomial fitting (Fig. 4c) and cross-wavelet analysis (Fig. S7) confirm a significant coherency within the ~80-year band. The covarying δ^{13} C and δ^{18} O values in YX120 record indicate that stalagmite δ^{18} O may also reflect regional hydroclimate changes on multidecadal to decadal timescales. Therefore, we interpret that changes in stalagmite δ^{18} O records in the mid-YRV can primarily reflect variations in EASM intensity and associated Meiyu rainfall, with negative δ^{18} O values related to strong EASM and lengthening of the Meiyu rainfall, and vice versa.

4.2. ENSO and EASM teleconnection on multidecadal timescales

The ENSO is a coupled tropical Pacific Ocean-atmosphere phenomenon that is the most dominant global source of interannual climate variability. Previously, both meteorological data and paleoclimatic records indicate that ENSO exerts substantial influence on the EASM strength and/or Meiyu rainfall over the mid-YRV on various timescales (Ding and Chan, 2005; Zhang et al., 2021). A composite stalagmite record from three caves over the mid-YRV indicates that centennial-scale hydroclimate variations are probably modulated by ENSO, with increased Meiyu rainfall corresponding to El Niño-like conditions (Zhang et al., 2021). A highresolution precipitation reconstruction based on pollen records from the mid-YRV also confirms that intensified EASM associated with El Niño-like conditions leads to long Meiyu season and increased precipitation along the mid-YRV (Cui et al., 2018). However, meteorological studies show a weakening of the EASM intensity and a decrease of Meiyu rainfall since the late 1970s (Guo et al., 2004; Tan, 2014; Ding et al., 2020), probably related to an anomalous warming in Niño3.4 SST (Li et al., 2013, Fig. 5a). In this study, we try to reconcile the differences in the ENSO-EASM relationship between modern and historical observations.

To assess the historical ENSO-EASM teleconnection, we compared the composite YX-HS $\delta^{18}O$ record with a unified ENSO proxy (UEP) extracted by Principal Component Analysis of 10 commonly used ENSO proxies (Fig. 5b; McGregor et al., 2010). Due to the different temporal resolution between the YX-HS record (0.2 yr on average) and UEP index (1 yr), we first resampled the YX-HS record to produce a uniform 1-year spacing and then applied the correlation coefficient and wavelet analyses on them. After applying an 11-year running mean, the YX-HS record shows a similarity (r = -0.30, n = 177, P < 0.01) with the UEP on decadal timescales during the interval from 1784-1970 AD (Fig. 5b and Fig. S8). To evaluate the significance of the correlation of the YX-HS record with UEP index, we generated 1000 Fourier based surrogate signals sharing statistical characteristics of the YX-HS original data using the Monte-Carlo approach (Theiler et al., 1992), and then calculated correlation between each pair of surrogates and UEP index. As a result, the correlation between the YX-HS and UEP index is statistically significant above the 0.01 level. The multidecadal

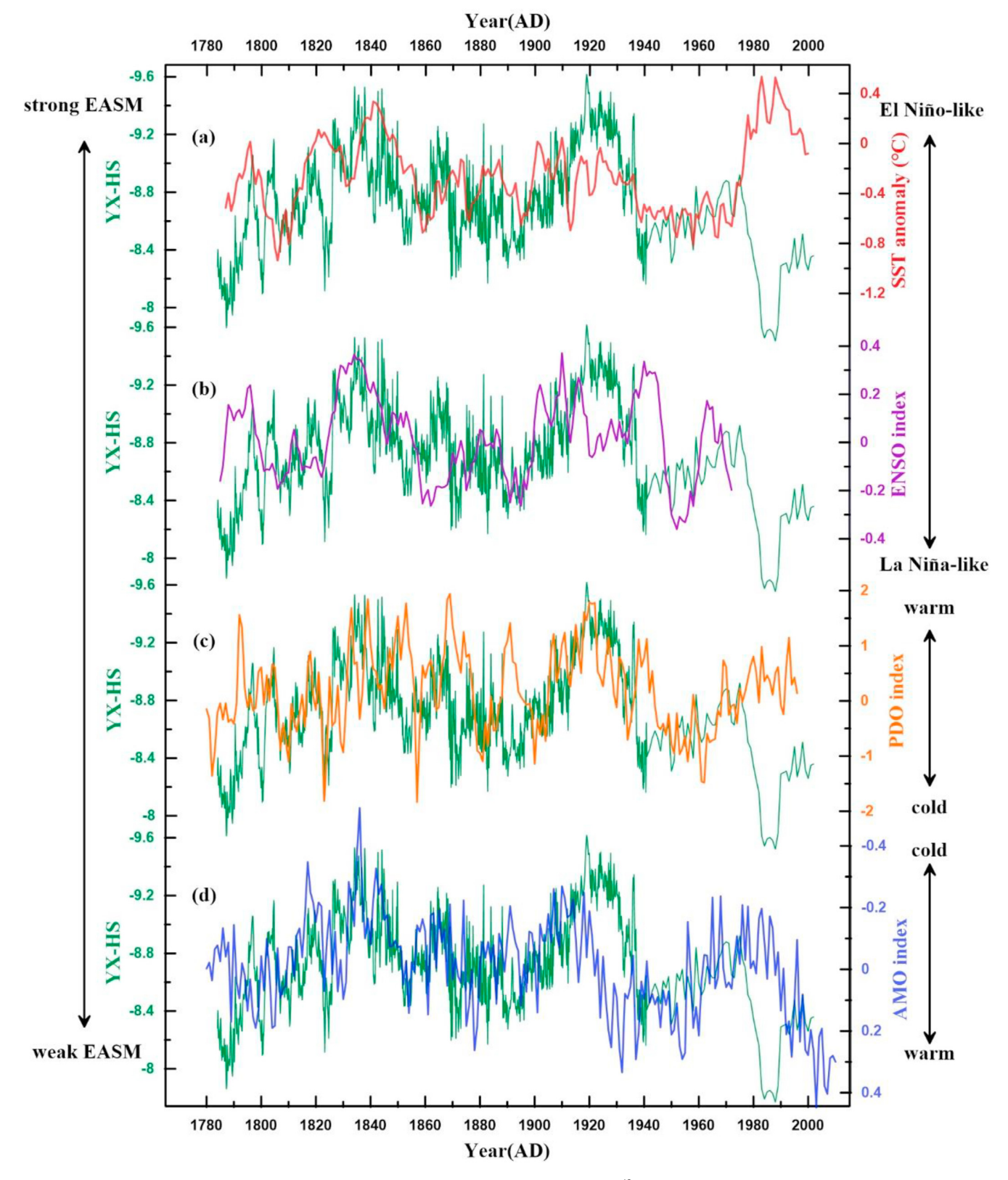


Fig. 5. Comparison of the EASM record with ENSO reconstructions, PDO index and AMO index. The YX-HS δ^{18} O record is in green. (a) Niño3.4 SST anomalies (dark red, 11-year running mean) relative to the mean of observed SSTs during 1971–2000 AD (Li et al., 2013); (b) UEP index (purple, 11-year running mean), revealed by Principal Component Analysis of 10 commonly used ENSO proxies (McGregor et al., 2010); (c) PDO index based on hydrologically sensitive Pinus flexilis tree-ring chronologies (orange, MacDonald and Case, 2005); (d) AMO index based on 46 annually resolved terrestrial proxy records (blue, Wang et al., 2017). (For interpretation of the references to colour in this figure legend, the reader is referred to the Web version of this article.)

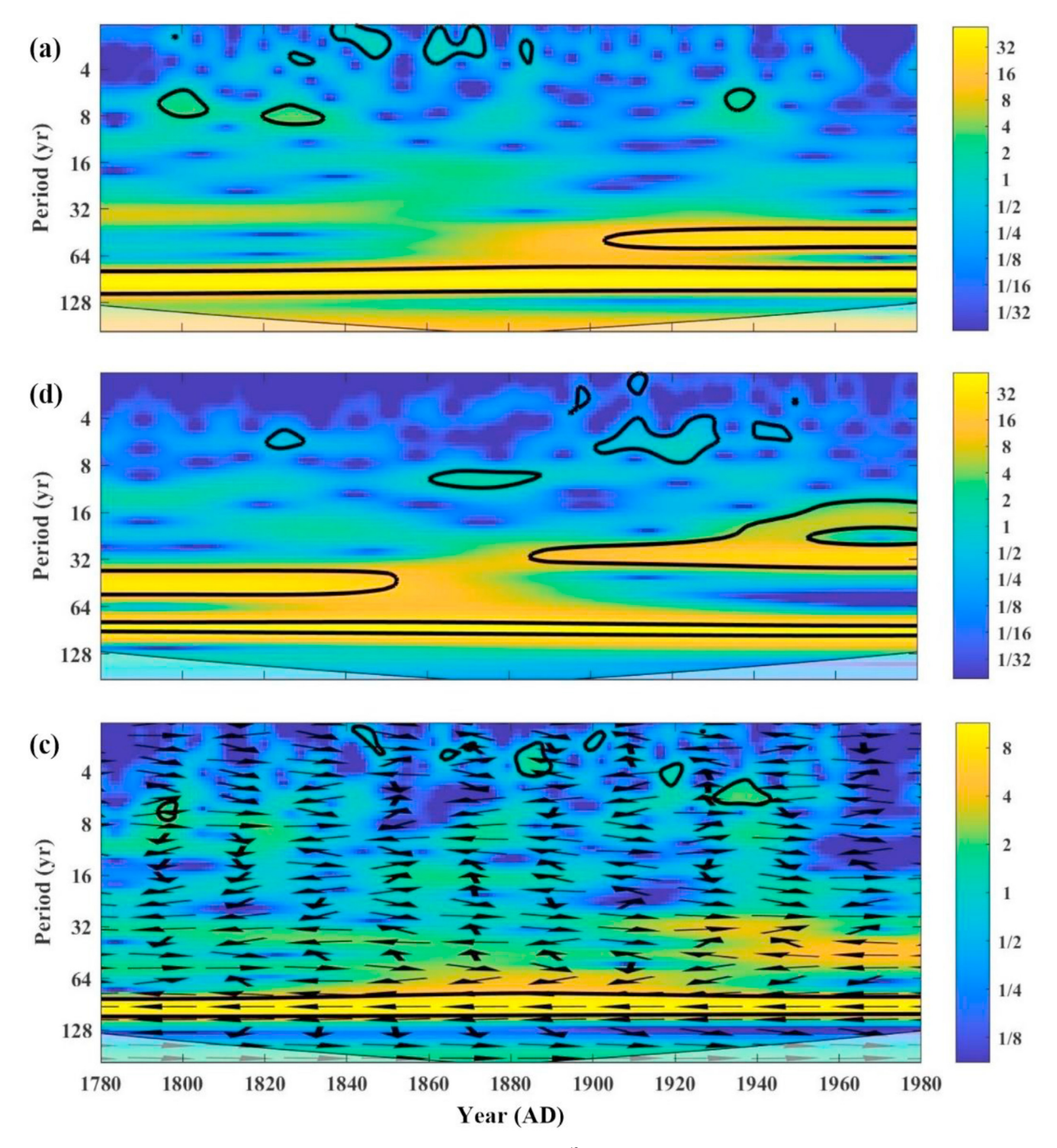


Fig. 6. The wavelet analyses of YX-HS record and ENSO index from 1784 to 1970 AD. The YX-HS δ^{18} O record was resampled to produce a 1-year temporal resolution. The continuous wavelet transforms (CWT) of YX-HS record (a) and UEP index (15-year running mean) (b) (McGregor et al., 2010) (c) The cross-wavelet analysis between YX-HS record and UEP index (with a uniform 1-yr temporal resolution). The 95% confidence level against red noise is shown as a thick contour. The black arrows (right/left) indicate the phase relation (in-/ anti-phase). The analysis was estimated on Matlab 2020a. The coherence package is available at: http://noc.ac.uk/using-science/crosswavelet-wavelet-coherence. (For interpretation of the references to colour in this figure legend, the reader is referred to the Web version of this article.)

oscillations in the two records are comparable. Wavelet and power spectral analyses of both proxies show a dominant periodicity of ~80 years (Fig. 6a and b; Fig. S9). The cross-wavelet analysis between the YX-HS record and UEP index confirms a close correlation

coherently at ~80 yr cyclicity (Fig. 6c). We also compared the YX-HS record with an ENSO reconstruction based on 2222 tree-ring chronologies from both the tropics and mid-latitudes in both hemispheres (Fig. 5a; Li et al., 2013), which was attested by high

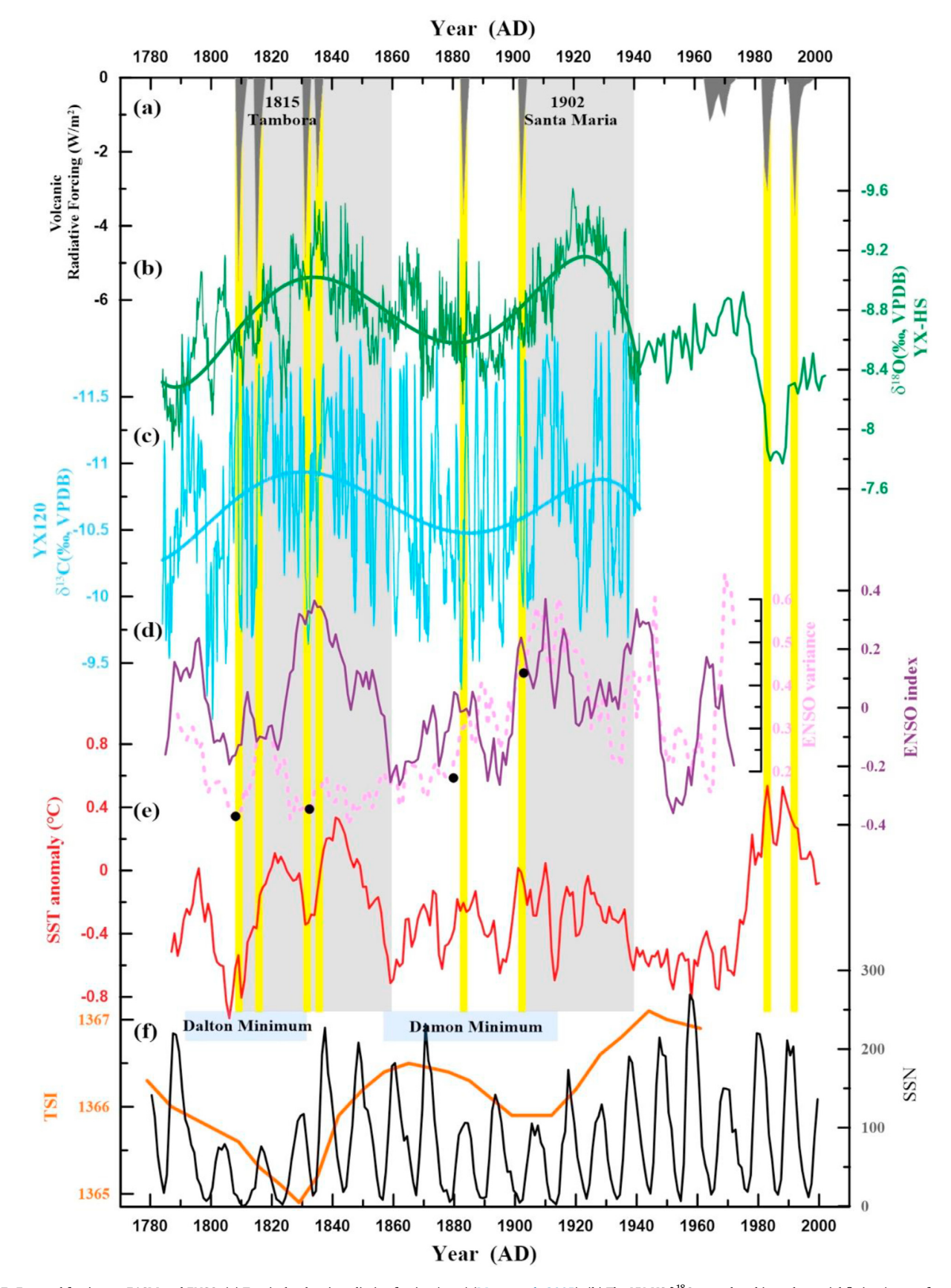


Fig. 7. External forcing on EASM and ENSO. (a) Tropical volcanic radiative forcing (gray) (Mann et al., 2005); (b) The YX-HS δ¹⁸O record and its polynomial fitting (green, from 1784 to 1941 AD); (c) YX120 δ¹³C record and its polynomial fitting (light blue); (d) UEP index (purple solid line, 11-year running mean) and its 11-year running window variance (light

correlations with equatorial Pacific corals (Cobb et al., 2003). The decadal-scale changes in EASM are closely linked to those in the Niño3.4 SST anomalies (Fig. 5a). The Pearson correlation coefficient between YX-HS record and ENSO reconstruction during 1784—1970 AD is $-0.40\ (n=177,\ significant\ above\ the\ 0.01\ level\ using\ the Monte-Carlo approach, 11-year running mean of both records). These results support the idea that multidecadal changes in the EASM are strongly related to ENSO-like states, with intensified EASM and lengthened Meiyu duration corresponding to El Niño-like conditions.$

The PDO, as a long-lived ENSO-like pattern of Pacific climate variability, is strongly related to ENSO changes on decadal timescales, with warm PDO phases corresponding to El Niño-like states. The multidecadal changes in our new EASM record are thus likely related to the shifts in PDO conditions. The multidecadal variability in the UEP is consistent with the 20th century variability of the PDO, as well as previously defined reconstructions of the PDO (McGregor et al., 2010). The close relationship between our YX-HS record and UEP suggests that the PDO probably exerts a decadal modulation effect on EASM and Meiyu duration in the mid-YRV (Fig. 5b). The YX-HS record was further compared with a PDO index based on hydrologically sensitive Pinus flexilis tree-ring chronologies from California and Alberta (MacDonald and Case, 2005, Fig. 5c). The Pearson correlation coefficient between YX-HS record and PDO index during 1784–1970 AD is -0.60 (n = 177, significant above the 0.01 level using the Monte-Carlo approach, 11-year running mean of both records). This high similarity reveals that enhanced EASM and lengthened Meiyu duration are largely related to the warm PDO phases and El Niño-like states, and vice versa, in consistent with the modeling results (Zhu et al., 2016; Liu et al., 2022). In addition, meteorological observations indicate that the AMO plays an important role in modulating the ENSO-EASM relationship, probably through the circum-global stationary baroclinic wave train (Si and Ding, 2016) and/or the westerly jets (Chiang et al., 2015). Comparison of the YX-HS record and the AMO index (Fig. 5d, Wang et al., 2017) shows a good correlation during 1784-1970 AD, with a correlation coefficient of 0.39 (n = 177, significant above the 0.01 level using the Monte-Carlo approach, 11year running mean of both records). This result indicates an enhanced (weakened) EASM corresponding to a cool (warm) phase of AMO. Furthermore, a linkage between the AMO and PDO was confirmed through the AMO-Northern Hemisphere teleconnection wave train (Si and Ding, 2016). Our observations, consistent with the model simulations (Zhu et al., 2016; Liu et al., 2022), confirm a close ENSO-EASM relationship on multidecadal timescale, probably concurrently modulated by PDO and AMO.

In conclusion, both observational data and modeling evidence indicate that multidecadal-scale oscillations in EASM and/or Meiyu rainfall over the mid-YRV are likely related to the internal climate variability, involving ENSO, PDO and AMO, in the course of natural climatic variability. However, the ENSO-EASM relationship has changed since the late 1970s, with weakened EASM and shortened Meiyu duration corresponding to El Niño-like conditions (Fig. 5a), which is also revealed by meteorological studies (Guo et al., 2004; Tan, 2014; Ding et al., 2020). As shown in Fig. 5a, the weakened EASM intensity and high Niño3.4 SST since the late 1970s were anomalous over the past 200 years, even over the past millennium (Cobb et al., 2003; Li et al., 2013), suggestive of a response to the

continuing global warming (Li et al., 2013; Ding et al., 2020).

4.3. External forcing on EASM and ENSO

Solar irradiance and explosive volcanic activity are both mechanisms that can alter the natural radiative forcing of the climate system. Previous studies refer to an ocean dynamical thermostat mechanism whereby the SST in the eastern equatorial Pacific varies negatively with changes in solar irradiance (Clement et al., 1996; Mann et al., 2005). Modeling studies also suggest that ENSO is sensitive to sulfate aerosol forcing associated with explosive volcanism (Pausata et al., 2015), but observational support for this effect remains challenging (Dee et al., 2020).

To assess solar and volcanic influence on internal climate variability, here we investigate the role of the external radiative forcing on ENSO-EASM coupling. Wavelet analyses and cross-wavelet analysis of the EASM record and UEP index show a coherent periodicity of ~80 years (Fig. 6c), close to the Gleissberg 88-year solar cycle (Peristykh and Damon, 2003). As shown in Fig. 7, however, the two multidecadal-scale oscillations in the EASM and ENSO proxies (McGregor et al., 2010; Li et al., 2013), corresponding to lengthening of Meiyu durations and El Niño-like conditions, do not respond to the well-known Dalton Minimum (1790-1830 AD) and Damon Minimum (1856-1913 AD) (Bard et al., 2000; Sharp, 2010). Thus, this result does not support a direct solar forcing on multidecadalscale ENSO-EASM relationship. We further test the tropical volcanic effect on changes in ENSO and EASM. Adams et al. (2003) demonstrated a significant multi-year El Niño-like response to explosive tropical volcanic forcing over the past several centuries. In this study, most of the large tropical volcanic eruptions over the past 200 years can induce El Niño-like states and intensify EASM, and likely promote an enhanced phase-synchronization of the ENSO and EASM oscillations (Fig. 7). As shown in Fig. 7d, the change points of ENSO variance are consistent with the tropical volcanic eruptions within the age uncertainties, supporting that volcanic forcing can induce a statistically significant change in the mean state of ENSO (McGregor et al., 2010). For the recent two eruptions, the anomalous El Niño-like conditions since the late 1970s may be caused by the combined effect of anthropogenic and volcanic forcing. In a recent study, Liu et al. (2022) analyzed long-term multi-proxy data and multi-model simulations and found that a volcano-induced El Niño and the associated warm pool air-sea interaction can intensify the EASM and increase precipitation over the Yangtze River. Therefore, these observations confirm that tropical volcanic eruptions tend to strengthen the El Niño-EASM relationship.

In addition to the direct radiative effect, which lasts 2–3 years, the ocean-atmosphere system likely sustained volcanic effect for several years after the eruptions, which affected the slow components of the climate system (Brönnimann et al., 2019). It is possible that two multidecadal-scale transitions in EASM and ENSO-like evolution, occurred around ~1815 and ~1902 AD, coincide with the year of the Tambora and Santa María eruptions (Fig. 7), respectively. After the two volcanic eruptions during the solar minima, Niño3.4 SST increased and EASM enhanced, and the ENSO-EASM coupling strengthened on multidecadal timescale. The multidecadal variability in the ENSO is also consistent with the variability of the PDO (Fig. 7d, McGregor et al., 2010). Thus, the

volcanic forcing on multidecadal-scale changes in EASM can be further modulated by shifts in PDO phases. It was supposed that the ENSO response to volcanic eruptions largely depend on different pre-eruption background states of equatorial Pacific SST (Pausata et al., 2015). Under equatorial eastern Pacific initial warming, the Pacific and trade winds anomalies favor El Niño-like anomalies after volcanic eruptions, whereas La Niña-like anomalies tend to occur following eruptions under eastern Pacific initial cooling (Zuo et al., 2021). Then, the ENSO modulates the EASM and associated rainfall over the mid-YRV through atmospheric teleconnection, such as the East Asian-Pacific teleconnection (Ding and Chan, 2005; Zuo et al., 2021). This result roughly implies an enhanced El Niño-like and strengthened ENSO-EASM coupling on multidecadal timescale following a large tropical volcanic eruption.

To sum up, we reveal that tropical volcanic eruptions may induce El Niño-like conditions and enhanced EASM, in consistent with previous proxy evidence and modeling results (Adams et al., 2003; Liu et al., 2022). However, the dynamic linkages between Tambora and Santa María eruptions and multidecadal oscillations in EASM and ENSO are complex, as the influence of other eruptions is not clear. Here, we provide a possibility and the relationship between internal multidecadal oscillations in climate and volcanic eruptions remains controversial (Dee et al., 2020; Mann et al., 2021).

5. Conclusion

In this study, we present a high-resolution EASM record from 1784–1958 AD, based on 2315 δ^{18} O measurements from two annually-laminated stalagmites (YX92 and YX120) in Yongxing Cave over the mid-YRV. The main conclusions are as follows:

Firstly, the EASM variations show significant multidecadal-scale oscillations over the past 200 years, with a dominant periodicity of ~80 years. The multidecadal-scale oscillations in EASM are related to ENSO, PDO and/or AMO, suggesting a decadal modulation of EASM by the internal climate variability. The anomalies in EASM and Niño3.4 SST since the late 1970s are likely influenced by the increased anthropogenic radiative forcing.

Secondly, our observations, in consistent with previous proxy evidence and modeling studies, indicate that tropical volcanic eruptions tend to induce El Niño-like conditions and strengthen the ENSO-EASM relationship. Two multidecadal transitions in ENSO and EASM records are probably related to the eruptions of Tambora (1815 AD) and Santa María (1902 AD), respectively. These observations reveal that the internal multidecadal oscillations in climate are potentially modulated by tropical volcanic eruptions, especially during the solar minima.

In conclusion, our findings reveal that both external forcing and internal climate variability play an important role in driving the decadal-scale EASM variations during natural climatic variability. A comprehensive analysis of the expanded paleoclimate data and model simulations is expected to further test and refine these findings. This is helpful for model simulations to better understand and predict the climate response to the global warming.

Credit author statement

K.Z. and **J.Z.** designed the research and experiments; **K.Z.**, **J.Z.** and **Y.W.** wrote the manuscript, which was edited by all of the coauthors; **S.C.** and **Y.C.** provided the cave sample; **H.C.** and **R.L.E.** did the ²³⁰Th dating work; **X.K.**, **Y.L.** and **L.P.** contributed to oxygen isotope measurements. All authors discussed the results and provided input to the manuscript and technical aspects of the laboratory analyses.

Declaration of competing interest

The authors declare that they have no known competing financial interests or personal relationships that could have appeared to influence the work reported in this paper.

Data availability

The data used to sustain the results of this work are included in the article and its supplementary material files.

Acknowledgements

We thank Editor Dr. Miryam Bar-Matthews and three anonymous reviewers for their constructive comments. This work was supported by National Natural Science Foundation of China (Grants 42071105, 41931178), the U.S. National Science Foundation (Grant 1702816), the Project Funded by the Priority Academic Program Development of Jiangsu Higher Education Institutions (Grant 164320H116), Jiangsu Province "Qinglan Project" (2020) and the 111 Program of China (Grant D19002).

Appendix A. Supplementary data

Supplementary data to this article can be found online at https://doi.org/10.1016/j.quascirev.2022.107720.

References

- Adams, J., Mann, M., Ammann, C., 2003. Proxy evidence for an El Niño-like response to volcanic forcing. Nature 426, 274–278. https://doi.org/10.1038/nature02101.
- Anet, J.G., Muthers, S., Rozanov, E.V., Raible, C.C., Stenke, A., Shapiro, A.I., Brönnimann, S., Arfeuille, F., Brugnara, Y., Beer, J., Steinhilber, F., Schmutz, W., Peter, T., 2014. Impact of solar versus volcanic activity variations on tropospheric temperatures and precipitation during the Dalton Minimum. Clim. Past 10, 921–938. https://doi.org/10.5194/cp-10-921-2014.
- Baldini, J., McDermott, F., Baker, A., Baldini, L., Mattey, D., Railsback, L., 2005. Biomass effects on stalagmite growth and isotope ratios: a 20th century analogue from Wiltshire, England. Earth Planet Sci. Lett. 240, 486–494. https:// doi.org/10.1016/j.epsl.2005.09.022.
- Bard, E., Raisbeck, G., Yiou, F., Jouzel, J., 2000. Solar irradiance during the last 1200 years based on cosmogenic nuclides. Tellus Ser. B Chem. Phys. Meteorol. 52, 985–992. https://doi.org/10.3402/tellusb.v52i3.17080.
- Brönnimann, S., Franke, J., Nussbaumer, S.U., Zumbühl, H.J., Steiner, D., Trachsel, M., Hegerl, G.C., Schurer, A., Worni, M., Malik, A., Flückiger, J., Raible, C.C., 2019. Last phase of the Little Ice Age forced by volcanic eruptions. Nat. Geosci. 12, 650–656. https://doi.org/10.1038/s41561-019-0402-y.
- Chen, K., Ning, L., Liu, Z., Liu, J., Yan, M., Sun, W., Yuan, L., Lv, G., Li, L., Jin, C., Shi, Z., 2020. One drought and one volcanic eruption influenced the history of China: the late ming dynasty mega-drought. Geophys. Res. Lett. 47, e2020GL088124. https://doi.org/10.1029/2020gl088124.
- Cheng, H., Edwards, R., Sinha, A., Spötl, C., Yi, L., Chen, S., Kelly, M., Kathayat, G., Wang, X., Li, X., Kong, X., Wang, Y., Ning, Y., Zhang, H., 2016. The Asian monsoon over the past 640,000 years and ice age terminations. Nature 534, 640–646. https://doi.org/10.1038/nature18591.
- Chiang, J.C.H., Fung, I.Y., Wu, C.-H., Cai, Y., Edman, J.P., Liu, Y., Day, J.A., Bhattacharya, T., Mondal, Y., Labrousse, C.A., 2015. Role of seasonal transitions and westerly jets in East Asian paleoclimate. Quat. Sci. Rev. 108, 111–129. https://doi.org/10.1016/j.quascirev.2014.11.009.
- Clement, A., Seager, R., Cane, M., Zebiak, S., 1996. an Ocean dynamical thermostat. J. Clim. 9, 2190–2196. https://doi.org/10.1175/1520-0442(1996)009<2190: AODT>2.0.CO:2.
- Cobb, K., Charles, C., Cheng, H., Edwards, R., 2003. El Niño/Southern Oscillation and tropical Pacific climate during the last millennium. Nature 424, 271–276. https://doi.org/10.1038/nature01779.
- Cosford, J., Qing, H., Mattey, D., Eglington, B., Zhang, M., 2009. Climatic and local effects on stalagmite δ¹³C values at Lianhua Cave, China. Palaeogeogr. Palaeoclimatol. Palaeoecol. 280, 235—244. https://doi.org/10.1016/j.palaeo.2009.05.020.
- Cui, A., Ma, C., Zhao, L., Tang, L., Jia, Y., 2018. Pollen records of the little ice age humidity flip in the middle Yangtze River catchment. Quat. Sci. Rev. 193, 43–53. https://doi.org/10.1016/j.quascirev.2018.06.015.
- Dee, S., Cobb, K., Emile-Geay, J., Ault, T., Edwards, R., Cheng, H., Charles, C., 2020. No consistent ENSO response to volcanic forcing over the last millennium. Science 367, 1477–1481. https://doi.org/10.1126/science.aax2000.
- Ding, Y., Chan, J.C.L., 2005. The East Asian summer monsoon: an overview.

- Meteorol. Atmos. Phys. 89, 117–142. https://doi.org/10.1007/s00703-005-0125-7
- Ding, Y., Liang, P., Liu, Y., Zhang, Y., 2020. Multiscale variability of Meiyu and its prediction: a new review. J. Geophys. Res. Atmos. 125, e2019JD031496. https:// doi.org/10.1029/2019jd031496.
- Ding, Y., Si, D., Liu, Y., Wang, Z., Liu, Y., Zhao, L., Song, Y., 2018. On the characteristics, driving forces and inter-decadal variability of the East Asian summer monsoon. Chin. J. Atmos. Sci. 42, 533–558. https://doi.org/10.3878/j.issn.1006-9895.1712.17261 (in Chinese with English abstract).
- Dorale, J., Liu, Z., 2009. Limitations of Hendy Test criteria in judging the paleoclimatic suitability of speleothems and the need for replication. J. Cave Karst Stud. 71, 73–80.
- Duan, W., Ruan, J., Luo, W., Li, T., Tian, L., Zeng, G., Zhang, D., Bai, Y., Li, J., Tao, T., Zhang, P., Baker, A., Tan, M., 2016. The transfer of seasonal isotopic variability between precipitation and drip water at eight caves in the monsoon regions of China. Geochem. Cosmochim. Acta 183, 250–266. https://doi.org/10.1016/i.gca.2016.03.037.
- Edwards, R., Chen, J., Wasserburg, G., 1987. ²³⁸U-²³⁴U-²³⁰Th-²³²Th systematics and the precise measurement of time over the past 500,000 years. Earth Planet Sci. Lett. 81, 175–192.
- Emile-Geay, J., Cane, M., Seager, R., Kaplan, A., Almasi, P., 2007. El Niño as a mediator of the solar influence on climate. Paleoceanography 22, PA3210. https://doi.org/ 10.1029/2006pa001304.
- Fairchild, I.J., Smith, C.L., Baker, A., Fuller, L., Spötl, C., Mattey, D., McDermott, F., E.I.M.F, 2006. Modification and preservation of environmental signals in speleothems. Earth Sci. Rev. 75, 105–153. https://doi.org/10.1016/ i.earscirev.2005.08.003.
- Fohlmeister, J., Voarintsoa, N.R., Lechleitner, F., Boyd, M., Brandstätter, S., Jacobson, M., Oster, J., 2020. Main controls on the stable carbon isotope composition of speleothems. Geochem. Cosmochim. Acta 279, 67–87. https://doi.org/10.1016/j.gca.2020.03.042.
- Griffiths, M., Kimbrough, A., Gagan, M., Drysdale, R., Cole, J.E., Johnson, K., Zhao, J.-x., Cook, B., Hellstrom, J., Hantoro, W., 2016. Western Pacific hydroclimate linked to global climate variability over the past two millennia. Nat. Commun. 7, 11719. https://doi.org/10.1038/ncomms11719.
- Guo, Q.Y., Cai, J.N., Shao, X.M., Sha, W., 2004. Studies on the variations of East-Asian summer monsoon during AD 1873-2000. Chin. J. Atmos. Sci. 28, 206–215. https://doi.org/10.3878/j.issn.1006-9895.2004.02.04 (in Chinese with English abstract).
- He, L., Hu, C., Huang, J., Xie, S., Wang, Y., 2009. Characteristics of large-scale circulation of East Asian monsoon indicated by oxygen isotope of stalagmites. Quat. Sci. 29, 950–956. https://doi.org/10.3969/j.issn.1001-7410.2009.05.12 (in Chinese with English abstract).
- Hellstrom, J., 2006. U–Th dating of speleothems with high initial ²³⁰Th using stratigraphical constraint. Quat. Geochronol. 1, 289–295. https://doi.org/10.1016/j.quageo.2007.01.004.
- Hendy, C.H., 1971. Hendy, C. H. Isotopic geochemistry of speleothems—I. Calculation of effects of different modes of formation on isotopic composition of speleothems and their applicability as palaeoclimatic indicators. Geochem. Cosmochim. Acta 35, 801–824. https://doi.org/10.1016/0016-7037(71)90127-X. Geochim. Cosmochim. Acta 35, 801-824.
- Hu, C., Henderson, G., Huang, J., Xie, S., Sun, Y., Johnson, K.R., 2008a. Quantification of Holocene Asian monsoon rainfall from spatially separated cave records. Earth Planet Sci. Lett. 266, 221–232. https://doi.org/10.1016/j.epsl.2007.10.015.
- Hu, C., Henderson, G., Huang, J., Zhenghong, C., Kathleen, J., 2008b. Report of a three-year monitoring programme at Heshang Cave, Central China. Int. J. Speleol. 37, 143–151. https://doi.org/10.5038/1827-806X.37.3.1.
- Jiang, T., Zhang, Q., Zhu, D., Wu, Y., 2006. Yangtze floods and droughts (China) and teleconnections with ENSO activities (1470–2003). Quat. Int. 144, 29–37. https://doi.org/10.1016/j.quaint.2005.05.010.
- Johnson, K., Hu, C., Belshaw, N., Henderson, G., 2006. Seasonal trace-element and stable-isotope variations in a Chinese speleothem: the potential for highresolution paleomonsoon reconstruction. Earth Planet Sci. Lett. 244, 394–407. https://doi.org/10.1016/j.epsl.2006.01.064.
- Li, J., Chen, X., Cook, E., Morales, M., Christie, D., Johnson, N., Chen, F., D'Arrigo, R., Fowler, A., Gou, X., Fang, K., 2013. El Niño modulations over the past seven centuries. Nat. Clim. Change 3, 822–826. https://doi.org/10.1038/nclimate1936.
 Li, X., Cui, X., He, D., Liao, J., Hu, C., 2018. Evaluation of the Heshang Cave stalagmite
- Li, X., Cui, X., He, D., Liao, J., Hu, C., 2018. Evaluation of the Heshang Cave stalagmite calcium isotope composition as a paleohydrologic proxy by comparison with the instrumental precipitation record. Sci. Rep. 8, 2615. https://doi.org/10.1038/ s41598-018-20776-5.
- Liang, Y., Zhao, K., Edwards, R.L., Wang, Y., Shao, Q., Zhang, Z., Zhao, B., Wang, Q., Cheng, H., Kong, X., 2020. East Asian monsoon changes early in the last deglaciation and insights into the interpretation of oxygen isotope changes in the Chinese stalagmite record. Quat. Sci. Rev. 250, 106699. https://doi.org/10.1016/j.quascirev.2020.106699.
- Liu, F., Gao, C., Chai, J., Robock, A., Wang, B., Li, J., Zhang, X., Huang, G., Dong, W., 2022. Tropical volcanism enhanced the East Asian summer monsoon during the last millennium. Nat. Commun. 13, 3429. https://doi.org/10.1038/s41467-022-31108-7
- Liu, Y.H., Henderson, G.M., Hu, C.Y., Mason, A.J., Charnley, N., Johnson, K.R., Xie, S.C., 2013. Links between the east asian monsoon and north atlantic climate during the 8,200 year event. Nat. Geosci. 6, 117–120. https://doi.org/10.1038/ngeo1708.
- MacDonald, G., Case, R., 2005. Variations in the pacific decadal oscillation over the past millennium. Geophys. Res. Lett. 32, L08703. https://doi.org/10.1029/

- 2005GL022478.
- Man, W., Zhou, T., Jungclaus, J., 2014. Effects of large volcanic eruptions on global summer climate and East Asian monsoon changes during the last millennium: analysis of MPI-ESM simulations. J. Clim. 27, 7394–7409. https://doi.org/ 10.1175/ICLI-D-13-00739.1.
- Mann, M., Cane, M., Zebiak, S., Clement, A., 2005. Volcanic and solar forcing of the tropical pacific over the past 1000 years. J. Clim. 18, 447–456. https://doi.org/ 10.1175/ICLI-3276.1.
- Mann, M., Steinman, B., Brouillette, D., Miller, S., 2021. Multidecadal climate oscillations during the past millennium driven by volcanic forcing. Science 371, 1014–1019. https://doi.org/10.1126/science.abc5810.
- McDermott, F., 2004. Palaeo-climate reconstruction from stable isotope variations in speleothems: a review. Quat. Sci. Rev. 23, 901–918. https://doi.org/10.1016/ j.quascirev.2003.06.021.
- McGregor, S., Timmermann, A., Timm, O., 2010. A unified proxy for ENSO and PDO variability since 1650. Clim. Past Discuss 6, 1–17. https://doi.org/10.5194/cpd-5-2177-2009
- Mudelsee, M., 2003. Estimating pearson's correlation coefficient with bootstrap confidence interval from serially dependent time series. Math. Geol. 35, 651–665. https://doi.org/10.1023/B:MATG.0000002982.52104.02.
- Mudelsee, M., 2009. Break function regression. Eur. Phys. J. Spec. Top. 174, 49–63. https://doi.org/10.1140/epjst/e2009-01089-3.
- Orland, I., Edwards, R., Cheng, H., Kozdon, R., Warner, M., Valley, J., 2015. Direct measurements of deglacial monsoon strength in a Chinese stalagmite. Geology 43, 555–558. https://doi.org/10.1130/G36612.1.
- Owen, R.A., Day, C.C., Hu, C.Y., Liu, Y.H., Pointing, M.D., Blättler, C.L., Henderson, G.M., 2016. Calcium isotopes in caves as a proxy for aridity: modern calibration and application to the 8.2 kyr event. Earth Planet Sci. Lett. 443, 129–138. https://doi.org/10.1016/j.epsl.2016.03.027.
- Pausata, F.S., Chafik, L., Caballero, R., Battisti, D.S., 2015. Impacts of high-latitude volcanic eruptions on ENSO and AMOC. Proc. Natl. Acad. Sci. U.S.A. 112, 13784–13788. https://doi.org/10.1073/pnas.1509153112.
- Peristykh, A.N., Damon, P.E., 2003. Persistence of the Gleissberg 88-year solar cycle over the last ~12,000years: evidence from cosmogenic isotopes. J. Geophys. Res. 108. https://doi.org/10.1029/2002ja009390. SSH 1-1-SSH 1-15.
- Richards, D., Dorale, J., 2003. Uranium-series chronology and environmental applications of speleothems. Rev. Mineral. Geochem. 52, 407–460. https://doi.org/10.2113/0520407.
- Sharp, G., 2010. Are uranus & Neptune responsible for solar grand minima and solar cycle modulation? Int. J. Astrophys. Astron. 3, 260–273. https://doi.org/10.4236/ ijaa.2013.33031.
- Si, D., Ding, Y., 2016. Oceanic forcings of the interdecadal variability in East Asian summer rainfall. J. Clim. 29, 7633–7649. https://doi.org/10.1175/jcli-d-15-0792.1.
- Singh, M., Raghavan, K., Goswami, B., D. C, A., Panickal, S., Vellore, R., Ag, P., Narayanasetti, S., Venkataraman, C., Donner, R., 2020. Fingerprint of volcanic forcing on the ENSO-Indian monsoon coupling. Sci. Adv. 6, eaba8164. https:// doi.org/10.1126/sciadv.aba8164.
- Tan, M., 2014. Circulation effect: response of precipitation $\delta^{18}O$ to the ENSO cycle in monsoon regions of China. Clim. Dynam. 42. https://doi.org/10.1007/s00382-013-1732-x.
- Tan, M., Baker, A., Genty, D., Smith, C., Esper, J., Cai, B., 2006. Applications of stalagmite laminae to paleoclimate reconstructions: comparison with dendro-chronology/climatology. Quat. Sci. Rev. 25, 2103–2117. https://doi.org/10.1016/j.quascirev.2006.01.034.
- Theiler, J., Eubank, S., Longtin, A., Galdrikian, B., Doyne Farmer, J., 1992. Testing for nonlinearity in time series: the method of surrogate data. Physica D 58, 77–94. https://doi.org/10.1016/0167-2789(92)90102-S.
- Wang, J., Yang, B., Ljungqvist, F., Luterbacher, J., Osborn, T., Briffa, K., Zorita, E., 2017. Internal and external forcing of multidecadal Atlantic climate variability over the past 1,200 years. Nat. Geosci. 10, 512–517. https://doi.org/10.1038/ ngeo2962.
- Wang, Q., Wang, Y., Zhao, K., Chen, S., Liu, D., Zhang, Z., Huang, W., Yang, S., Liang, Y., 2018. The transfer of oxygen isotopic signals from precipitation to drip water and modern calcite on the seasonal time scale in Yongxing Cave, central China. Environ. Earth Sci. 77, 474. https://doi.org/10.1007/s12665-018-7607-z.
- Wang, Y., Hu, C., Ruan, J., Johnson, K., 2020. East Asian precipitation 8¹⁸O relationship with various monsoon indices. J. Geophys. Res. Atmos. 125. https://doi.org/ 10.1029/2019[D032282.
- Wang, Y.J., Cheng, H., Edwards, R.L., An, Z.S., Wu, J.Y., Shen, C.C., Dorale, J.A., 2001. A high-resolution absolute-dated late Pleistocene Monsoon record from Hulu Cave, China. Science 294, 2345–2348. https://doi.org/10.1126/science.1064618.
- Yang, B., Qin, C., Osborn, T., Trouet, V., Ljungqvist, F., Esper, J., Schneider, L., Grießinger, J., Büntgen, U., Rossi, S., Dong, G., Yan, M., Ning, L., Wang, J., Wang, X., Wang, S., Luterbacher, J., Cook, E., Stenseth, N.C., 2021. Long-term decrease in Asian monsoon rainfall and abrupt climate change events over the past 6,700 years. Proc. Natl. Acad. Sci. U.S.A. 118, e2102007118. https://doi.org/10.1073/pnas.2102007118.
- Yuan, D., Cheng, H., Edwards, R., Dykoski, C., Kelly, M., Zhang, M., Qing, J., Lin, Y., Wang, Y., Wu, J., Dorale, J., An, Z., Cai, Y., 2004. Timing, duration, and transitions of the last interglacial asian monsoon. Science 304, 575–578. https://doi.org/10.1126/science.1091220.
- Zhang, H., Griffiths, M., Chiang, J., Kong, W., Wu, S., Atwood, A., Huang, J., Cheng, H., Ning, Y., Xie, S., 2018. East Asian hydroclimate modulated by the position of the westerlies during Termination I. Science 362, 580–583. https://doi.org/10.1126/

science.aat9393.

- science.aat9393.

 Zhang, J., Zhao, K., Wang, Y., Kong, X., Shao, X., Liang, Y., Cui, Y., Cheng, H., Edwards, R.L., Shao, Q., 2021. Modulation of centennial-scale hydroclimate variations in the middle Yangtze River Valley by the East Asian-Pacific pattern and ENSO over the past two millennia. Earth Planet Sci. Lett. 576, 117220. https://doi.org/10.1016/j.epsl.2021.117220.

 Zhang, P., Cheng, H., Edwards, R., Chen, F., Wang, Y., Yang, X., Liu, J., Tan, M., Wang, X., Liu, J., An, C., Dai, Z., Zhou, J., Zhang, D., Jia, J., Jin, L., Johnson, K., 2008.
- A test of climate, sun, and culture relationships from an 1810-year Chinese cave record. Science 322, 940—942. https://doi.org/10.1126/science.1163965.

 Zhu, Y., Wang, T., Ma, J., 2016. Influence of internal decadal variability on the
- summer rainfall in Eastern China as simulated by CCSM4. Adv. Atmos. Sci. 33, 706–714. https://doi.org/10.1007/s00376-016-5269-x.

 Zuo, M., Man, W., Zhou, T., 2021. Dependence of global monsoon response to volcanic eruptions on the background oceanic states. J. Clim. 34, 8273–8289. https://doi.org/10.1175/jcli-d-20-0891.1.